Modeling and Simulation of New Encoding Schemes for High-Speed UHF RFID Communication

Sang-Hyun Mo, Ji-Hoon Bae, Chan-Won Park, Hyo-Chan Bang, and Hyung Chul Park

In this paper, we present novel high-speed transmission schemes for high-speed ultra-high frequency (UHF) radio-frequency identification communication. For high-speed communication, tags communicate with a reader using a high-speed Miller (HS-Miller) encoding and multiple antennas, and a reader communicates with tags using extended pulse-interval encoding (E-PIE). E-PIE can provide up to a two-fold faster data rate than conventional pulse-interval encoding. Using HS-Miller encoding and orthogonal multiplexing techniques, tags can achieve a two- to three-fold faster data rate than Miller encoding without degrading the demodulation performance at a reader. To verify the proposed transmission scheme, the MATLAB/Simulink model for high-speed backscatter based on an HS-Miller modulated subcarrier has been designed and simulated. The simulation results show that the proposed transmission scheme can achieve more than a 3 dB higher BER performance in comparison to a Miller modulated subcarrier.

Keywords: RFID, passive tag, high-speed Miller encoding, multi-antenna, extended pulse-interval encoding.

I. Introduction

Radio-frequency identification (RFID), a non-contact automatic recognition technology, is a technology for recognizing electronic tags on products using a radio frequency. RFID technology can be classified, in a broad sense, into a passive RFID system and an active RFID system. In a passive RFID system, a tag is not supplied with power from a battery; hence, it must communicate with a reader based on backscatter by generating self-power in response to a carrier signal from the reader. A passive RFID system can be used for various applications in comparison to barcodes because it can provide information on individual objects without requiring the use of batteries in tags. There has been a significant amount of research on improving passive RFID system technologies. Previous work [1]–[2] has mainly focused on developing an efficient algorithm to enhance inventory efficiency. In [3]–[5], many kinds of receiver structures for demodulating backscattered tag signals were introduced. In addition, with the remarkable development in low-power semiconductor technologies, inexpensive RFID tags are becoming a reality [6]–[7]. However, most research has focused on demodulation, protocol algorithms for readers, and implementation issues related to tags.

These days, high-memory passive RFID tags are required for applications that need to store data beyond an identification number. For example, manufacturing engineers for the aerospace and car industries have seen benefits in storing inspection, birth, and repair records. In addition, according to an increase in the amount of data handled, file management and security services for RFID are required [8]–[9]. Nevertheless, existing passive RFID systems have problems in terms of performance and transmission speed. Traditional

Manuscript received Aug. 9, 2014; revised Jan. 29, 2015; accepted Feb. 3, 2015.

This work was supported by ETRI R&D Program [15ZC1200, The Development of passive RFID technology for improvement of reliability and high speed with large scaled memory] funded by the Government of Korea.

Sang-Hyun Mo (shmo@etri.re.kr), Ji-Hoon Bae (baejh@etri.re.kr), Chan-Won Park (cwp@etri.re.kr), and Hyo-Chan Bang (bangs@etri.re.kr) are with the IT Convergence Technology Research Laboratory, ETRI, Daejeon, Rep. of Korea.

Hyung Chul Park (corresponding author, hcpark@seoultech.ac.kr) is with the Department of Electronic and IT Media Engineering, Seoul National University of Science and Technology, Seoul, Rep. of Korea.

passive RFID tags with a Miller-modulated subcarrier based on the ISO/IEC 18000-63 international standard [10] have data rates of up to 320 kbps, which is insufficient for reading a large amount of data in a tag memory. For this reason, there is a necessity to develop new modulation techniques for increasing the data rate of RFID tags.

In some previous studies, high–data rate RFID systems have been studied [11]–[13]. In [11] and [12], M-ary quadrature amplitude modulated (M-QAM) backscatter was proposed. With M-QAM backscatter, tags can transmit $\log_2 M$ data bits per symbol period; however, tags can achieve only a 10^{-3} BER performance with E_b/N_0 between 9 dB and 11 dB. There also exists an implementation issue regarding the accuracy difference between the ideal and measured impedance values. In [13], a digital RF-transmitting scheme with a 1 Mbps data rate is described, but this transmitter needs to be battery powered. To overcome this weakness, we propose a new transmission scheme to increase the data rate of a tag without degrading the demodulation performance or requiring additional battery power. In this paper, we present two-dimensional bi-orthogonal signaling and orthogonal multiplexing techniques for passive RFID tags. The data rate of the proposed scheme is two to three times faster than a Miller modulated subcarrier with the same occupied bandwidth.

The READ command in the ISO/IEC 18000-63 international standard [10] allows a reader to read part of or all of a tag memory. When WordCount equals zero in the READ command, a tag should reply the contents of the chosen memory bank starting at WordPtr and ending at the end of the bank. However, according to an increase in the read data size of a tag memory, the probability of the packet error is also increased. Therefore, when a reader tries to read the contents in a high-memory tag, the reader should repeatedly send a READ command with the proper WordCount until obtaining all information in the memory. For this reason, the data rate of a reader is also important to increase the reading speed of the tag memory. We propose a new encoding scheme for reader-to-tag communication that can provide a two-fold faster data rate in comparison to pulse-interval encoding (PIE). It can contribute to an improvement in both the reading and inventory speeds.

The rest of this paper is organized as follows. Section II presents a new encoding scheme and decoding algorithm for forward link communication. In Section III, the modulation and demodulation signal model for a high-speed Miller (HS-Miller) modulated subcarrier are described. In Section IV, we describe the transmitter and receiver structures for the proposed transmission scheme based on MATLAB/Simulink, as well as providing the experimental results. In Section V, some concluding remarks are provided.

II. Proposed Extended Pulse-Interval Encoding (E-PIE) Scheme

1. Data Encoding

To increase the data rate of a reader, a reader encodes the reader command using E-PIE. E-PIE uses four kinds of symbol waveforms and can transmit two bits per symbol waveform. In Fig. 1, E-PIE symbol waveforms are described. E-PIE symbol waveforms are composed of a signal having a different length with high and low values. High values represent the transmitted CW, and low values represent the attenuated CW. The Tari is the basic time reference unit for reader-to-tag signaling, and here, it represents the duration of symbol-0 and symbol-1. The reader can communicate using Tari values within the range of 6.25 μs to 25 μs. A 1.5 Tari value is used as the duration of symbol-2 and symbol-3. The conventional PIE scheme encodes one bit per symbol waveform based on the information of different symbol durations. The symbol duration of data-0 is 1 Tari, and the symbol duration of data-1 is between 1.5 Tari and 2 Tari. However, the E-PIE scheme encodes two bits per symbol waveform based on two different lengths of high and low values. For example, the first data bit determines the total symbol duration between 1 Tari and 1.5 Tari, and the second data bit determines the length of the low value between 0.5 Tari and 0.265 Tari. RF parameters for generating E-PIE symbol waveforms follow the current ISO/IEC 18000-63 standard [10]; thus, when we apply the E-PIE scheme, there will be no problems with tag operations.

2. Data Decoding

Theoretically, both PIE and E-PIE have almost an error-free

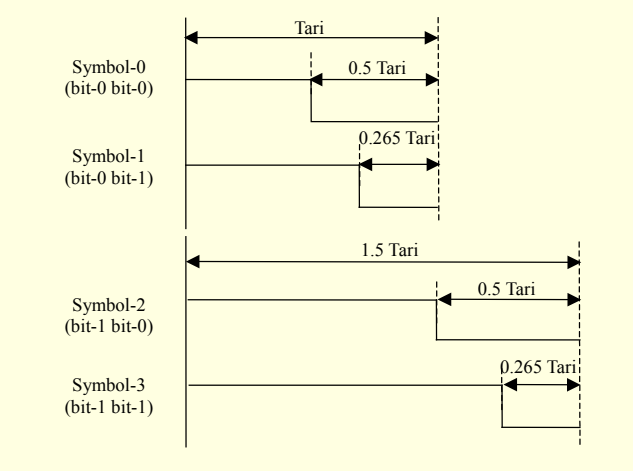

Fig. 1. Proposed extended pulse-interval encoding (E-PIE) symbol waveforms.

ETRI Journal, Volume 37, Number 2, April 2015
http://dx.doi.org/10.4218/etrij.15.2314.0111

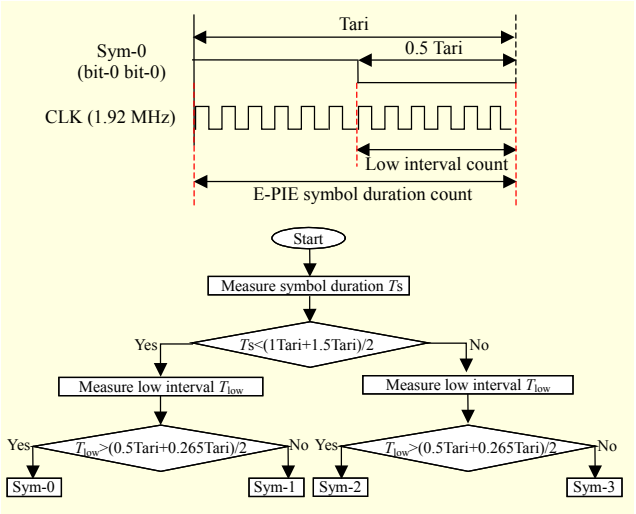

Fig. 2. Decoding algorithm for E-PIE symbols.

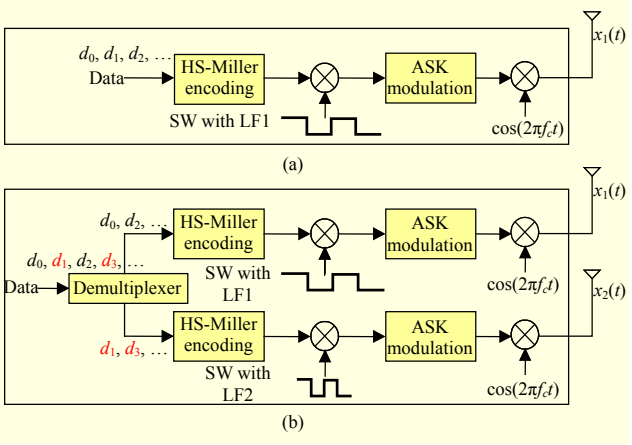

Fig. 3. Block diagram of a tag modulator based on an HS-Miller subcarrier: (a) single HS-Miller subcarrier and (b) double HS-Miller subcarriers.

demodulation performance because the important factor for a tag operation is not the sensitivity of the tag but the received power from the reader. As long as the tag can wake up, it can have a sufficient signal-to-noise ratio (SNR) value (that is, almost 100 dB) and therefore there will be no bit error when a tag demodulates E-PIE symbols.

To decode the E-PIE signal, only one more counter is required to measure the low interval length, and a low-clock rate can be used. A decoding algorithm for E-PIE symbols is described in Fig. 2. First, a tag needs to measure the symbol duration. A tag interprets the received E-PIE symbol as symbol-0 (Sym-0) and symbol-1 (Sym-1) when the measured symbol duration is shorter than the average symbol duration. After that, the tag again compares the measured low interval length with the average low interval length. When the measured low interval length is longer than the average low interval length, the tag finally determines the received E-PIE symbol to be symbol-0. A decoding algorithm for other E-PIE symbols is similar to symbol-0.

III. Proposed HS-Miller Encoding Scheme

1. Modulation of HS-Miller Subcarrier Signals

A tag communicates with a reader using backscatter modulation in which the tag switches the reflection coefficient in accordance with the data signal. A tag encodes the backscattered data as the HS-Miller of a subcarrier. For high-speed communication, a tag uses up to two transmit antennas. When a tag transmits the backscattered data using two antennas, a tag generates double HS-Miller subcarriers, where each subcarrier has a different link frequency (LF). A block diagram of a tag modulator is shown in Fig. 3. The backscattered bits are converted into 4-ary symbols, and the symbols are encoded using the symbol waveforms in the 4-ary bi-orthogonal signal set. This signal set will be explained later. For generating the HS-Miller subcarrier signal, the output waveform of the HS-Miller encoder is multiplied by a square wave (SW) with the defined LF, which is M-times the symbol rate, $1/T$. Therefore, an HS-Miller subcarrier signal shall contain exactly M subcarrier cycles per symbol duration, T. The HS-Miller subcarrier signal is modulated by an ASK modulator and up-converted using a received carrier signal from the reader.

The transmitted signal, $x_i(t)$, of the ith tag antenna is given by

$$x_i(t) = \sum_{m=-\infty}^{\infty} s_{i,j}(t - mT_i) w_i(t) \cos(2\pi f_c t), \quad (1)$$

where m is the mth order of the HS-Miller symbols, $s_{i,j}(t)$ is the jth symbol waveform in the 4-ary bi-orthogonal signal set for the ith HS-Miller subcarrier ($j \in \{1, 2, 3, 4\}$), $w_i(t)$ is an SW for the ith HS-Miller subcarrier, and f_c is the carrier frequency.

The N bi-orthogonal signal waveform set can be obtained from an original orthogonal set of $N/2$ signals by augmenting it with the negative of each signal. Therefore, the N signal waveforms are represented as the following set:

$$s_j(t) \in \{s_1(t), s_2(t), \ldots, s_{N/2}(t), -s_1(t), -s_2(t), \ldots, -s_{N/2}(t)\}. \quad (2)$$

The original orthogonal waveforms have to satisfy the following orthogonal condition:

$$\int_0^T s_k(t) s_l(t)\, dt = \begin{cases} E_s & \text{if } k = l, \\ 0 & \text{if } k \neq l, \end{cases} \quad (3)$$

where k and $l \in \{1, 2, \ldots, N/2\}$. Such a set of bi-orthogonal waveforms can be represented as a set of $N/2$ dimensional orthogonal vectors. That is,

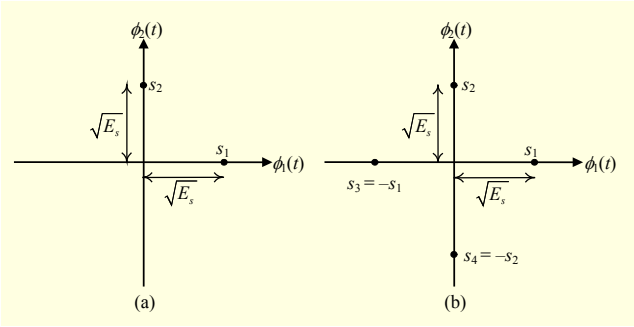

Fig. 4. Signal constellations for Miller and HS-Miller signals: (a) orthogonal signal for Miller and (b) 4-ary bi-orthogonal signal for HS-Miller.

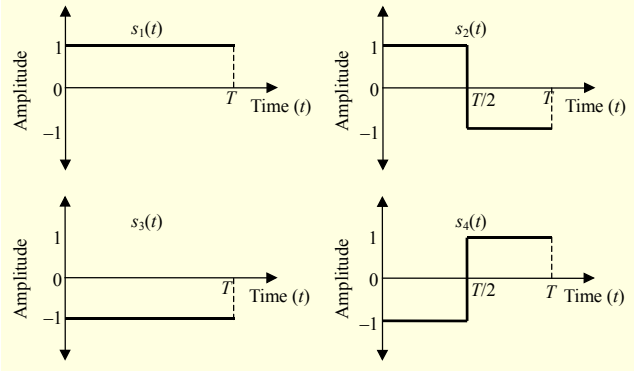

Fig. 5. Basis waveforms for HS-Miller encoding.

$$s_1 = (\sqrt{E_s},\ 0,\ 0,\ \ldots,\ 0),\ \ldots,\ s_{N/2} = (0,\ 0,\ 0,\ \ldots,\sqrt{E_s}),$$
$$s_{(N/2)+1} = (-\sqrt{E_s},\ 0,\ 0,\ \ldots,\ 0),\ \cdots,\ s_N = (0,\ 0,\ 0,\ \ldots,-\sqrt{E_s}). \quad (4)$$

Figure 4 illustrates the signal constellations corresponding to $N = 4$ bi-orthogonal signals for HS-Miller encoding and two-dimensional orthogonal signals for Miller encoding.

In this paragraph, HS-Miller encoding and a method for generating an HS-Miller subcarrier are explained. In the HS-Miller encoding process, every two bits are mapped to HS-Miller symbols, and HS-Miller symbols are encoded using 4-ary bi-orthogonal waveforms. In comparison to Miller encoding ($M = 4$), HS-Miller encoding can transmit data two-times faster than Miller encoding during the same symbol period T. For generating an HS-Miller subcarrier, an HS-Miller encoded waveform is multiplied by SW at M-times the symbol rate. Figure 5 shows bi-orthogonal waveforms for HS-Miller encoding, and HS-Miller subcarrier signals are described in Fig. 6.

When a tag transmits backscattered data using orthogonal double subcarriers, it can achieve a much faster data rate. To satisfy the orthogonal characteristic between two subcarriers, the LF of one HS-Miller subcarrier is L-times faster than the other subcarrier. Therefore, using an orthogonal multiplexing technique, there is no performance degradation at the reader.

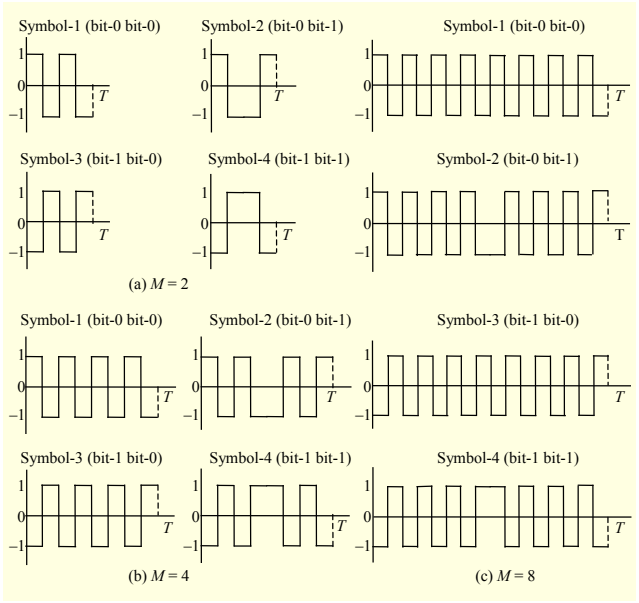

Fig. 6. HS-Miller subcarrier signals: (a) $M = 2$, (b) $M = 4$, and (c) $M = 8$.

Table 1. Data rates of Miller subcarrier and HS-Miller subcarrier.

Encoding type	M	Assumed LF (kHz)	Data rate (kbps)
Single HS-Miller	2	640	640
	4	640	320
	8	640	160
Double HS-Miller	2	640/320	960
	4	640/320	480
	8	640/320	240
Miller	2	640	320
	4	640	160
	8	640	80

In Table 1, we briefly compare the data rate of an HS-Miller subcarrier with that of a Miller subcarrier. The data rate of each HS-Miller subcarrier can be calculated as

$$\text{Data rate} = (\text{LF}/M)\times 2. \quad (5)$$

In the following section, we describe the demodulation structures and methods for HS-Miller subcarrier signals.

2. Demodulation of HS-Miller Subcarrier Signals

For demodulation of an HS-Miller subcarrier signal, the maximum a posterior probability (MAP) detector is required. Assume that an HS-Miller subcarrier signal is used to transmit backscattered data through an AWGN channel, and without

consideration of a low-pass filter and other RF component effects, the received signal, $r(t)$, is simply defined by

$$r(t) = s_j(t)w(t) + n(t) \quad \text{for } 0 \le t \le T, \tag{6}$$

where $n(t)$ is white Gaussian noise with a power spectrum of $N_0/2$ watts/hertz , $s_j(t)$ is the jth symbol waveform in the N bi-orthogonal signal set ($j \in \{1, 2, \dots, N\}$), and $w(t)$ is an SW for generating an HS-Miller subcarrier. The optimum MAP detector can be implemented using signal correlators for an original orthogonal set of $N/2$ signals. The received signal $r(t)$ is cross-correlated with each of the $N/2$ reference orthogonal signal waveforms, and correlator outputs are sampled at a sampling rate of $1/T$. The sampled signal r_i is given by

$$\begin{aligned} r_i &= \int_0^T r(t)s_i(t)w(t)\,\mathrm{d}t \quad \text{for } i = 1, 2, \dots, N/2 \\ &= \begin{cases} E + n_i & \text{if } j = i, \\ -E + n_i & \text{if } j = i + N/2, \\ n_i & \text{else,} \end{cases} \end{aligned} \tag{7}$$

where

$$n_i = \int_0^T n(t)s_i(t)w(t)\,\mathrm{d}t \quad \text{for } i = 1, 2, \dots, N/2 \tag{8}$$

and E is the symbol energy for each signal waveform. An example of the optimum MAP detector for an HS-Miller subcarrier signal is described in Fig. 7. The optimum MAP detector observes four correlator outputs and chooses the one with the largest magnitude. Next, the detector determines the HS-Miller symbols according to the sign of the chosen correlator output. The decision rule can be written as

$$\begin{aligned} \hat{s}_i &= \arg\max_i \{|r_i|\} \text{ and } r_i > 0, \\ \hat{s}_{i+(N/2)} &= \arg\max_i \{|r_i|\} \text{ and } r_i < 0 \qquad (i = 1, 2, \dots, N/2). \end{aligned} \tag{9}$$

We compare the probability of a bit error occurring between the Miller subcarrier and HS-Miller subcarrier schemes. The Miller subcarrier scheme uses two-dimensional orthogonal waveforms to encode the transmit data. In two-dimensional orthogonal signaling, the probability of a bit error can be expressed as

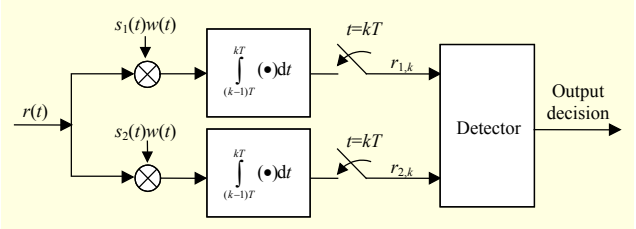

Fig. 7. Optimum MAP detector structure for HS-Miller subcarrier signal.

$$\begin{aligned} P_{\text{e,Miller}} &= \frac{1}{\sqrt{2\pi}} \int_{-\infty}^{\infty} Q(x) e^{-\left(x - \sqrt{2E_b/N_0}\right)^2/2}\,\mathrm{d}x \\ &= Q\left(\sqrt{E_b/N_0}\right), \end{aligned} \tag{10}$$

where E_b is bit energy.

Now, we consider the probability of a bit error for an HS-Miller subcarrier signal. The conditional probability of a correct decision for equally likely messages is as follows. We assume that $s_1(t)$ is transmitted.

$$\begin{aligned} p(r_1 \mid s_1(t),\, r_1 > 0) &= \Pr(-r_1 < \text{all } r_j < r_1 : j \ne 1 \mid s_1(t),\, r_1 > 0) \\ &= \{\Pr(-r_1 < \text{all } r_j < r_1 \mid s_1(t),\, r_1 > 0)\}^{(N/2)-1} \\ &= \left[\int_{-r_1/\sqrt{N_0/2}}^{r_1/\sqrt{N_0/2}} e^{-r^2/2}\,\mathrm{d}r\right]^{(N/2)-1}. \end{aligned} \tag{11}$$

Averaging over the probability density function of r_1, we can derive the correct decision probability as

$$\begin{aligned} p(r_1 \mid s_1(t)) = \int_{r_1=0}^{\infty} &\left[\int_{-\infty}^{r_1/\sqrt{N_0/2}} e^{-r^2/2}\,\mathrm{d}r\right]^{(N/2)-1} \\ &\times \frac{1}{\pi\sqrt{2N_0}} e^{-(r_1 - E)^2/N_0}\,\mathrm{d}r_1, \end{aligned} \tag{12}$$

where $N_0/2$ is the variance of the Gaussian noise n_i, and E is the symbol energy for the $s_1(t)$ waveform. For an HS-Miller subcarrier scheme, given $N = 4$, the probability of a bit error can be written as

$$P_{\text{e,HS-Miller}} \approx Q\left(\sqrt{2E_b/N_0}\right). \tag{13}$$

Thus, the HS-Miller subcarrier scheme achieves an SNR that is about 3 dB better than that of the Miller subcarrier scheme for the same given BER. Moreover, basis waveforms for FM0 encoding are the same as Miller encoding. HS-Miller can have a demodulation performance that is about 3 dB better than that of FM0 encoding.

IV. Design of Simulation Model and Experimental Results

1. MATLAB/Simulink Model for Tag-to-Reader Communication Based on HS-Miller Subcarrier

In this section, we present a MATLAB/Simulink model for the modulation and demodulation of HS-Miller subcarrier signals. This simulation model can be used for examining the characteristics of the transmitted tag signal and the demodulation performance of the receiver structure. Figure 8 shows a top-level block diagram of the tag-to-reader communication model based on an HS-Miller subcarrier. The simulation model consists of a transmitter, an AWGN channel,

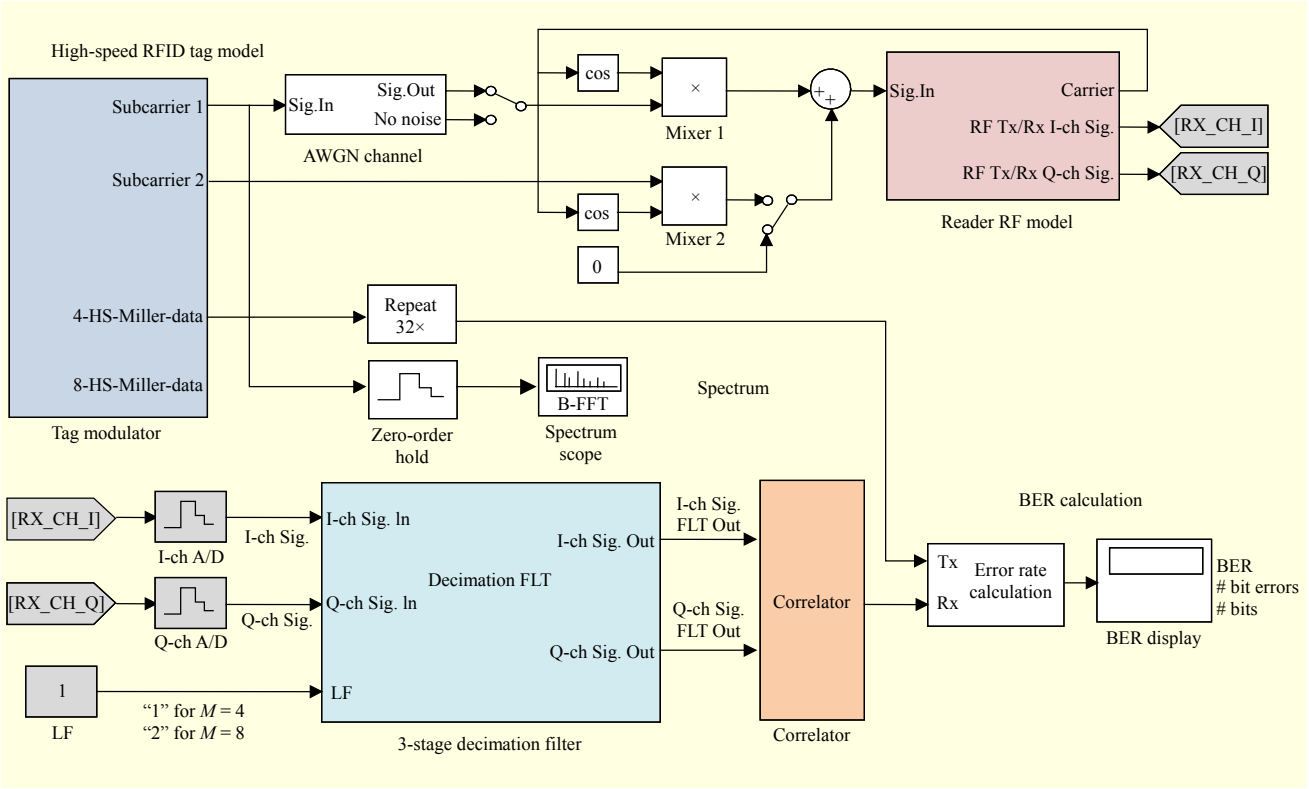

Fig. 8. Top-level block diagram of the tag-to-reader MATLAB/Simulink model based on HS-Miller subcarrier.

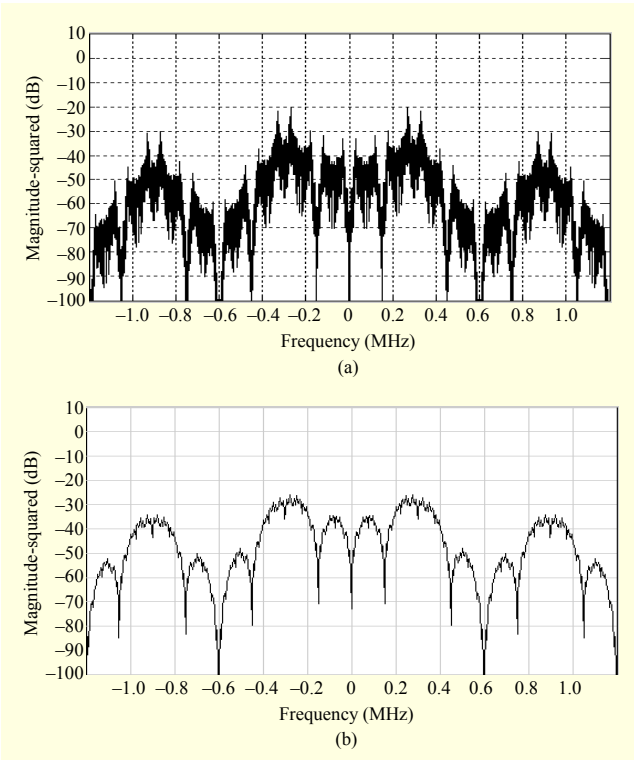

Fig. 9. Frequency response of the transmitted signal: (a) Miller subcarrier (M = 4, LF = 300 kHz) and (b) HS-Miller subcarrier (M = 4, LF = 300 kHz).

and a receiver. The transmitter block includes a bit data generator, an HS-Miller encoder, and an HS-Miller subcarrier generator and is able to select parameter M, the number of subcarriers, and the LF of each subcarrier. Figure 9 shows the frequency spectrums of a Miller subcarrier signal and an HS-Miller subcarrier signal. In particular, the frequency spectrum of an HS-Miller subcarrier signal does not have a dc component; thus, the receiver is not affected by the dc-offset noise.

$$\int_0^T s_i(t)w(t)\,dt = 0 \quad \text{for } i = 1, 2, \ldots, N. \tag{14}$$

As shown in Fig. 9, the frequency response of an HS-Miller subcarrier is very similar to the frequency response of a Miller subcarrier; therefore, the same analog and digital filters for Miller decoding can be used at the transmitter and receiver. In addition, our proposed scheme can be fitted based on the regulation of the channel signaling defined in the ISO/IEC 18000-63 international standard [10], and can be used for a dense reader environment. The AWGN channel model can be set up for both the SNR value and the existence of noise. After passing through the AWGN channel, the baseband signal of the HS-Miller subcarrier is up-converted by the received carrier signal from the reader. At the receiver block, the RF module down-converts the received RF signal. The down-converted signal is filtered by a low-pass filter and over-sampled by a digital-to-analog converter. The baseband modem module

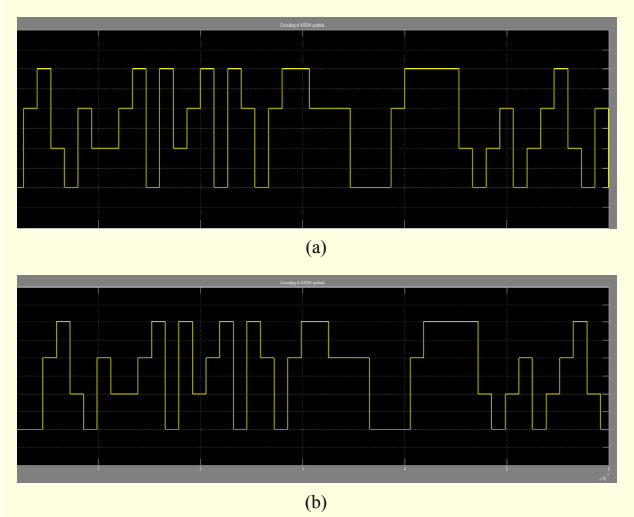

Fig. 10. Input and recovered streams of the HS-Miller symbols: (a) source HS-Miller symbols and (b) recovered HS-Miller symbols.

consists of a decimation filter and a correlator for an HS-Miller symbol decision. A decimation filter is used for down-sampling the received baseband signal according to the LF and sampling frequency. The correlator calculates the cross-correlation energy of both the received baseband signal and the reference HS-Miller subcarrier signal and provides the output to the HS-Miller symbol decoder. As we explained in Section III, the HS-Miller symbol decoder compares the correlator outputs and determines the HS-Miller symbol. The outputs from both the random bit generator block and the HS-Miller decoding block are simultaneously sent to the error rate calculation block, and the BER is computed. As shown in Fig. 10, the HS-Miller symbols are well recovered from the transmitted HS-Miller symbol with AWGN using the correlator and symbol decoder in our designed simulation model. Compared with the HS-Miller source symbols, which have four kinds of quantization levels, the recovered HS-Miller symbols simply have a time delay owing to several filtering processes.

Our tag-to-reader link layer simulation model provides the facilities to simulate and test a passive RFID system at a high level of abstraction. In the following section, we evaluate the performance of the proposed scheme using our MATLAB/Simulink model.

2. Experimental Results

In this section, we provide experimental results demonstrating the effectiveness of our proposed transmission scheme for high-speed tag-to-reader communication. We compare the BER performance of a single HS-Miller subcarrier scheme to both the FM0 and the Miller subcarrier scheme. In addition, we

Table 2. Simulation parameters for double subcarriers.

Parameter	Description
Encoding	Double HS-Miller
LF (kHz)	Double subcarrier: LF1 300, LF2 600 Double subcarrier with interference: LF2 450, LF2 600

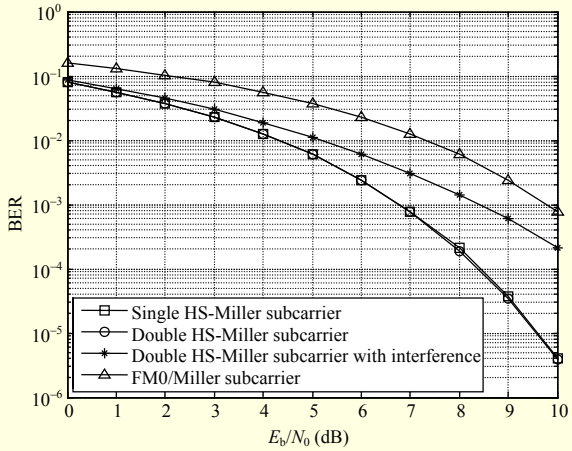

Fig. 11. BER comparison between HS-Miller subcarrier scheme and FM0/Miller subcarrier scheme.

evaluate the demodulation performance for a double HS-Miller subcarrier scheme under specific LF conditions in which the LF of one subcarrier is twice as fast as that of the other subcarrier. Figure 11 shows the BER performance of the HS-Miller subcarrier scheme in the presence of AWGN. We compare the BER of the single HS-Miller subcarrier scheme to the theoretical BER of both the FM0 and the Miller subcarrier. The simulation results show that the single HS-Miller subcarrier scheme can achieve about a 3 dB higher BER performance than the Miller subcarrier at the same E_b/N_0 and that it has a BER of 10^{-5} at an E_b/N_0 of 10 dB. We also evaluated the demodulation performance for the double HS-Miller subcarrier scheme. To demonstrate the advantage of orthogonal multiplexing techniques, we assume two types of LFs for double subcarriers. In Table 2, the LFs of the double HS-Miller subcarriers are defined. In Fig. 11, a BER comparison between the single HS-Miller and double HS-Miller subcarriers schemes is shown. The simulation results show that the double HS-Miller subcarrier provides the same performance as the single HS-Miller subcarrier when LF2 is twice as fast as LF1. Under this condition, these subcarriers are orthogonal; thus, there is no performance degradation at the receiver caused by mutual interference. The orthogonal multiplexing condition for the double HS-Miller subcarrier

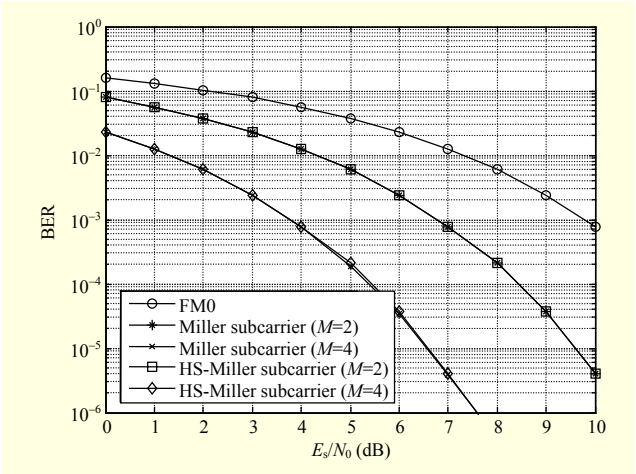

Fig. 12. BER comparison between HS-Miller subcarrier scheme and FM0/Miller subcarrier scheme from the point of view of required E_s/N_0.

scheme can be written as

$$\text{LF1}/\text{LF2} = M \text{ or } \text{LF2}/\text{LF1} = N, \quad (15)$$

where M and N are integers. When HS-Miller subcarriers are transmitted with LF1 at 600 kHz and LF2 at 450 kHz, about a 1 dB performance degradation is caused by mutual interference. To reject such interference, an interference rejection filter is required at the receiver.

The data rate of FM0 encoding in ISO/IEC 18000-63 [10] is up to 640 Kbps, and the data rate of the Miller subcarrier is significantly slower than that of FM0 by a factor of two, four, or eight. However, a Miller subcarrier is widely used in real-field applications because a Miller subcarrier requires less E_s/N_0 for the given BER and is more suitable for a dense reader environment. To overcome the slow data rate of the Miller subcarrier, the proposed HS-Miller subcarrier is a highly useful solution for increasing the data rate of a tag without degrading the demodulation performance. In Fig. 12, the HS-Miller subcarrier has the same demodulation performance as the Miller subcarrier in terms of the required E_s/N_0; however, it can achieve a two- to three-fold faster data rate than the Miller subcarrier.

V. Conclusion

In this paper, we presented new encoding methods suitable for high-speed UHF RFID communications. In forward link communication, a reader encodes the transmitted data using E-PIE. E-PIE can achieve a two-fold faster data rate than PIE, and only one more counter is required to decode E-PIE symbols at the tag. In backward link communication, the designed subcarrier signals are modulated by M-state bi-orthogonal basis waveforms and are transmitted using up to two antennas. The proposed HS-Miller subcarrier scheme can improve the data rates remarkably in comparison to a Miller subcarrier. For example, a single HS-Miller subcarrier scheme can achieve a two-fold faster data rate than a Miller subcarrier when the number of subcarrier cycles per symbol is four. Moreover, the frequency spectrum of HS-Miller subcarrier signals is very similar to that of Miller subcarrier signals; thus, HS-Miller subcarrier signals satisfy the channel signaling regulations defined in the ISO/IEC 18000-63 standard. In addition, our proposed scheme is easy to implement. The tag complexity of a single HS-Miller subcarrier scheme is the same as that of a Miller subcarrier; however, when a tag uses double HS-Miller subcarriers, the RF block of the tag complexity is increased owing to the use of two load modulators. The reader complexity is the same in single subcarrier transmission, and the reader complexity of double HS-Miller subcarriers is slightly increased because the signal detection and synchronization blocks are the same as in a Miller subcarrier, although two demodulation blocks are required for double HS-Miller subcarriers. To demonstrate our proposed scheme, we developed a simulation model for high-speed backward link communication based on HS-Miller subcarriers. We utilized this simulation model using the MATLAB/ Simulink tool and simulated the BER performance in an AWGN channel. For the single HS-Miller subcarrier scheme, the simulation results indicate that a BER performance of 10^{-5} can be achieved at an E_b/N_0 of 10 dB and 9 dB, respectively. In addition, in double HS-Miller subcarrier transmission mode, the link frequencies for each subcarrier have to satisfy the orthogonal multiplexing condition, which is defined in (15), to achieve a faster data rate than a single subcarrier without degrading the performance. Likewise, the proposed scheme significantly improves the data rate, spectral efficiency, and BER performance in comparison to the Miller subcarrier scheme. Additional future work includes constructing a tag emulator that implements an HS-Miller subcarrier, and evaluating the real-world performance in a passive RFID environment.

References

[1] L. Kang et al., "DDC: A Novel Scheme to Directly Decode the Collisions in UHF RFID Systems," *IEEE Trans. Parallel Distrib. Syst.*, vol. 23, no. 2, Feb. 2012, pp. 263–270.

[2] C. Jin et al., "An Efficient Collision Detection Scheme for Generation-2 RFID Systems," *Int. J. Comput. Sci. Issues*, vol. 9, no. 1, Sept. 2012, pp. 29–39.

[3] J.-H. Bae et al., "Design of Reader Baseband Receiver Structure for Demodulating Backscattered Tag Signal in a Passive RFID

Environment," *ETRI J*., vol. 34, no. 2, Apr. 2012, pp. 147–158.
[4] I. Mayordomo et al., "Design and Implementation of a Long-Range RFID Reader for Passive Transponders," *IEEE Trans. Microw. Theory Techn*., vol. 57, no. 5, May 2009, pp. 1283–1290.
[5] S.-C. Jung et al., "A Reconfigurable Carrier Leakage Canceler for UHF RFID Reader Front-Ends," *IEEE Trans. Circuits Syst*., vol. 58, no. 1, Jan. 2011, pp. 70–76.
[6] V. Pillai et al., "An Ultra-Low-Power Long Range Battery/Passive RFID Tag for UHF and Microwave Bands with a Current Consumption of 700 nA at 1.5 V," *IEEE Trans. Circuits Syst*., vol. 54, no. 7, July 2007, pp. 1500–1512.
[7] H. Nakamoto et al., "Passive UHF RF Identification CMOS Tag IC Using Ferroelectric RAM in 0.35 μm Technology," *IEEE J. Solid-State Circuits*, vol. 42, no. 1, Jan. 2007, pp. 101–110.
[8] S. Choi et al., "A Fully Integrated CMOS Security-Enhanced Passive RFID Tag," *ETRI J*., vol. 36, no. 1, Feb. 2014, pp. 141–150.
[9] Y.S. Kang, D. Choi, and D.-J. Park, "Comments on an Improved RFID Security Protocol for ISO/IEC WD 29167–6," *ETRI J*., vol. 35, no. 1, Feb. 2013, pp. 170–172.
[10] ISO/IEC Std. 18000-63, *Information Technology - Radio Frequency Identification for Item Management - Part 63: Parameters for Air Interface Communication at 860 MHz to 960 MHz Type C*, ISO/IEC JTC1/SC 31, 2013.
[11] S.J. Thomas and M.S. Reynolds, "QAM Backscatter for Passive UHF RFID Tags," *IEEE Int. Conf. RFID*, Orlando, FL, USA, Apr. 14–16, 2010, pp. 210–214.
[12] S.J. Thomas and M.S. Reynolds, "A 96 Mbit/sec, 15.5 pJ/bit 16 QAM Modulator for UHF Backscatter Communication," *IEEE Int. Conf. RFID*, Orlando, FL, USA, Apr. 3–5, 2012, pp. 185–190.
[13] K. Suzuki, M. Ugajin, and M. Harada, "A 1 Mbps 1.6 μA Micro-Power Active-RFID CMOS LSI for 300 MHz Frequency Band," *IEEE/MTT-S Int. Microw. Symp*., Honolulu, HI, USA, June 3–8, 2007, pp. 571–574.

Sang-Hyun Mo received his BS and MS degrees in electronic and electrical engineering from Pohang University of Science and Technology (POSTECH), Rep. of Korea, in 2006 and 2008, respectively. Since 2008, he has been with the Electronics and Telecommunications Research Institute, Daejeon, Rep. of Korea, as a researcher. His current research interests include RFID systems, wireless communication systems, and modem designs for communication systems.

Ji-Hoon Bae received his BS degree in electronic engineering from Kyungpook National University, Daegu, Rep. of Korea, in 2000 and his MS degree in electrical engineering from Pohang University of Science and Technology (POSTECH), Rep. of Korea, in 2002. Since 2002, he has been with the Electronics and Telecommunications Research Institute, Daejeon, Rep. of Korea, as a senior researcher. In addition, since 2013, he has been pursuing his PhD degree in radar signal processing at POSTECH. His current research interests include modulation/demodulation of RFID readers, RFID systems, radar signal processing, array antennas, and optimization techniques.

Chan-Won Park received his BS and MS degrees in computer engineering from Kwangwoon University, Seoul, Rep. of Korea, in 1993 and 1996, respectively. From 1996 to 1999, he was a member of the ASIC engineering staff, KAIST IDEC, Daejeon, Rep. of Korea. Since 1999, he has been working at the Electronics and Telecommunications Research Institute (ETRI), Daejeon, Rep. of Korea and has been a director of the Smart Things Cognition Research Section at ETRI since 2010. His research interests include wireless LAN, IoT, M2M, RFID, and system of chips.

Hyo-Chan Bang received his BS and MS degrees in management engineering and industrial engineering from the Hokkaido Institute of Technology, Japan, in 1995 and 1997, respectively. In 2007, he completed a doctoral course in computer engineering from Chungnam National University, Daejeon, Rep. of Korea. From 1997 to 1999, he was an associate researcher at KT, Seoul, Rep. of Korea. In 2000, he joined the Electronics and Telecommunications Research Institute, Daejeon, Rep. of Korea, where he is currently a managing director of the IoT Convergence Research Department. His current research interests include platform, network, and device technologies related to IoT; distributed systems; mobile computing; and information security.

Hyung Chul Park received his BS, MS, and PhD degrees in electrical engineering from the Korea Advanced Institute of Science and Technology, Daejeon, Rep. of Korea, in 1996, 1998, and 2003, respectively. From 2003 to 2005, he was an SoC design engineer with Hynix Semiconductor, Seoul, Rep. of Korea. From 2005 to 2010, he was an assistant professor at Hanbat National University, Daejeon, Rep. of Korea. In 2010, he joined the faculty of

the Department of Electronic and IT Media Engineering, Seoul National University of Science and Technology, Rep. of Korea, where he is currently an associate professor. His current research interests include wireless modulation/demodulation algorithms, system design/implementation, and interface study between RF/IF stages and digital signal processing.

ETRI Journal, Volume 37, Number 2, April 2015
http://dx.doi.org/10.4218/etrij.15.2314.0111